






Cite this: *J. Mater. Chem. A*, 2024, 12, 7321

# High-power recycling: upcycling to the next generation of high-power anodes for Li-ion battery applications†

A. J. Green, <sup>ac</sup> E. H. Driscoll, <sup>\*abc</sup> P. A. Anderson, <sup>ac</sup> E. Kendrick <sup>bc</sup>  
and P. R. Slater <sup>\*ab</sup>

With the growing interest in niobium-based anodes for high-power lithium-ion batteries (LIBs), current chemistries (for this application) such as  $\text{Li}_4\text{Ti}_5\text{O}_{12}$  (LTO) anodes will be superseded, and as such an efficient and effective method of recycling needs to be considered. With this motivation, a potential upcycling route is proposed for LTO for the first time, such that Li is recovered as a salt and the titanium oxide (anatase) repurposed and used in the synthesis of current generation titanium-doped niobates. Using a variety of inorganic acids: HCl,  $\text{H}_2\text{SO}_4$  and  $\text{H}_3\text{PO}_4$  to achieve the proton-lithium exchange, the lithium was found to be completely leached from the LTO in the former 2 acids. The latter acid was found to give incomplete leaching, with the formation of  $\text{LiTiOPO}_4$ . In addition to the recovery of Li from the leached solution, we also investigated upcycling of the recovered  $\text{TiO}_2$  (anatase) into next generation anodes  $\text{TiNb}_2\text{O}_7$  and  $\text{Ti}_2\text{Nb}_{10}\text{O}_{29}$ . The rate performance of these upcycled materials was determined through the fabrication of Li half coin cells, where both materials were found to show excellent performance at high rates (219 (2)  $\text{mA h g}^{-1}$  and 168 (16)  $\text{mA h g}^{-1}$  at 2  $\text{A g}^{-1}$  for  $\text{TiNb}_2\text{O}_7$  and  $\text{Ti}_2\text{Nb}_{10}\text{O}_{29}$  respectively), highlighting the potential of this recycling strategy for LTO.

Received 6th December 2023  
Accepted 15th February 2024

DOI: 10.1039/d3ta07549d

rsc.li/materials-a

## Introduction

With the growing interest and demand for the electrification of infrastructure – in efforts to meet ‘Net Zero’ targets and to improve public health – there is a requirement for forward thinking with respect to second-life applications and the inevitability of recycling when Li-ion batteries (LIBs) do eventually become end-of-life.<sup>1–7</sup> There are a multitude of battery chemistries for rechargeable LIBs – from research scale to the commercial sector; in this body of work we focus on primarily recycling high-power anodes such as  $\text{Li}_4\text{Ti}_5\text{O}_{12}$  (LTO) towards current generation which consists of niobium-based electrodes.<sup>8,9</sup>

While graphite is often the anode of choice, the poor stability and inherent safety issues through high (dis)charging conditions resulting in dendrite formation, has led to alternative electrode chemistries to be sought after for high-power applications, one of which is LTO – a material with the spinel structure (Fig. 1) and originally evaluated for LIB anode

application over 30 years ago.<sup>10</sup> The LTO structure with a cubic close-packed anion arrangement, consists of lithium ions occupying 1/8 of the tetrahedral (8a) sites and partial occupancy of titanium and lithium on the octahedral (16d) site. The theoretical capacity of LTO stands at  $175 \text{ mA h g}^{-1}$  (lower than graphite at  $372 \text{ mA h g}^{-1}$ ), but while the material is inherently stable under fast charging conditions, the overall energy density suffers due to the high operating potential of *ca.* 1.55 V *vs.* Li metal (in contrast to graphite at *ca.* 0 V *vs.* Li metal).<sup>11–16</sup>

Despite this, the adoption of LTO batteries has not been hindered, and they are found extensively in applications where high-power and safety is required. In this respect, a report by Avicenne Energy has noted that 4% of the LIB anode market (standing at 235 000 tons) could be accounted for by LTO.<sup>17</sup> Another advantage of these cells is that the median lifetime is greater than other LIB technologies at 17.5 years (compared to LFP/NMC at 10 years).<sup>18</sup> However, there is now a significant shift within the research sector towards the next generation of high-power anodes in the form of niobium-based oxides.

The increased interest in niobium-based anodes, in particular those of the Wadsley–Roth block structures, is associated with the higher capacity *versus* LTO. In this respect, titanium-doped niobates, including  $\text{TiNb}_2\text{O}_7$ ,<sup>19–21</sup>  $\text{Ti}_2\text{Nb}_{10}\text{O}_{29}$ ,<sup>22</sup> and  $\text{TiNb}_{24}\text{O}_{62}$ ,<sup>23</sup> are of great interest. A wide range of other Wadsley–Roth niobium oxide phases have also been investigated.<sup>22,24–29</sup>

<sup>a</sup>School of Chemistry, University of Birmingham, Edgbaston, Birmingham, B15 2TT, UK. E-mail: e.h.driscoll@bham.ac.uk; p.r.slater@bham.ac.uk

<sup>b</sup>School of Metallurgy and Materials, University of Birmingham, Edgbaston, Birmingham, B15 2SE, UK

<sup>c</sup>The Faraday Institution, Harwell Campus, Didcot, OX11 0RA, UK

† Electronic supplementary information (ESI) available. See DOI: <https://doi.org/10.1039/d3ta07549d>



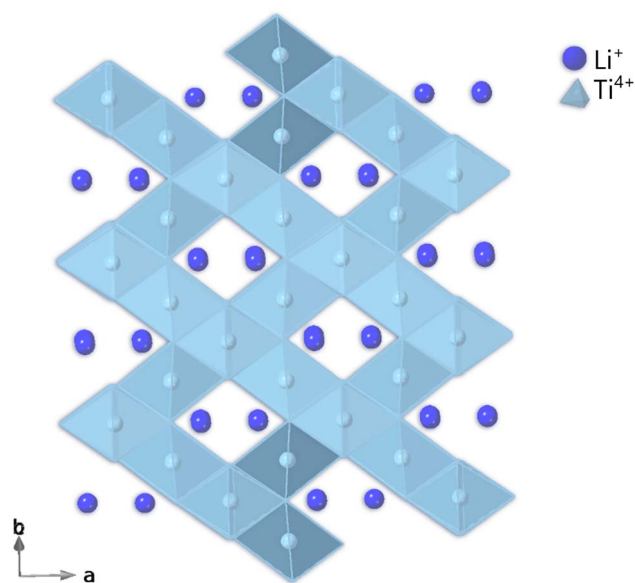


Fig. 1 Crystal structure of LTO.

These Wadsley–Roth phases adopt an oxygen deficient variation of the  $\text{ReO}_3$  crystal structure Fig. 2. The structures consist of corner-linked octahedra forming elongated blocks that extend infinitely in one dimension, creating  $(n \times m)_\infty$  networks of  $\text{MO}_6$  octahedra, with 'n' and 'm' representing the length and width of the block, respectively.<sup>30</sup> To accommodate the oxygen deficiency, crystallographic shear planes are introduced (Fig. 2), along with tetrahedral cations in certain systems. The open tunnels within the structure facilitate the diffusion of lithium ions during battery operation,<sup>31,32</sup> while the shear planes play

a crucial role in stabilizing the structure, as they prevent excessive volume expansion upon lithiation.<sup>33</sup> This helps to mitigate the degradation of the anode material, ensuring better performance and longevity of the battery. The size of the blocks in these structures is heavily influenced by the metal-to-oxygen ratio. A higher number of oxygens per metal atom allows for more connections between the corner-sharing octahedra, resulting in more substantial block sizes.<sup>34</sup>

In terms of recycling, work has focused on simple regeneration and reuse of LTO,<sup>35</sup> with no studies on potential upcycling to next generation Ti–Nb–O anodes with Li recovery. The latter is important, since, as of 2020, Li has been considered as a critical raw material by the European Commission highlighting the need to move away from LTO and prioritise Wadsley–Roth niobate anodes to reduce the Li content.<sup>36</sup> Li is a requirement for the cathode and electrolyte for a LIB and Li comprises ca. 6% of the composition of LTO by weight.<sup>37</sup> Thus, recycling LTO and upcycling it to the next generation niobate anodes will reduce the environmental impact produced by mining Li and the overall production of  $\text{CO}_2$ .<sup>37–40</sup> Niobium is also considered a critical material mainly due to its concentrated supply in Brazil.<sup>36,41,42</sup> However, reports have suggested that the projected supply of Nb is sufficient to cope with current and future demand for the next 500 years.<sup>43</sup>

As part of an investigation into LTO recycling, an approach for upcycling this current-generation anode material into the next-generation titanium-doped Wadsley–Roth anodes ( $\text{TiNb}_2\text{O}_7$  and  $\text{Ti}_2\text{Nb}_{10}\text{O}_{29}$  (Fig. 3)) has been developed in this paper. The approach involves an ion exchange process, where  $\text{Li}^+$  cations within the LTO are exchanged for protons from the acidic solution, thus enabling the recovery of anatase ( $\text{TiO}_2$ ) which is used in the synthesis of  $\text{TiNb}_2\text{O}_7$  and  $\text{Ti}_2\text{Nb}_{10}\text{O}_{29}$ . The

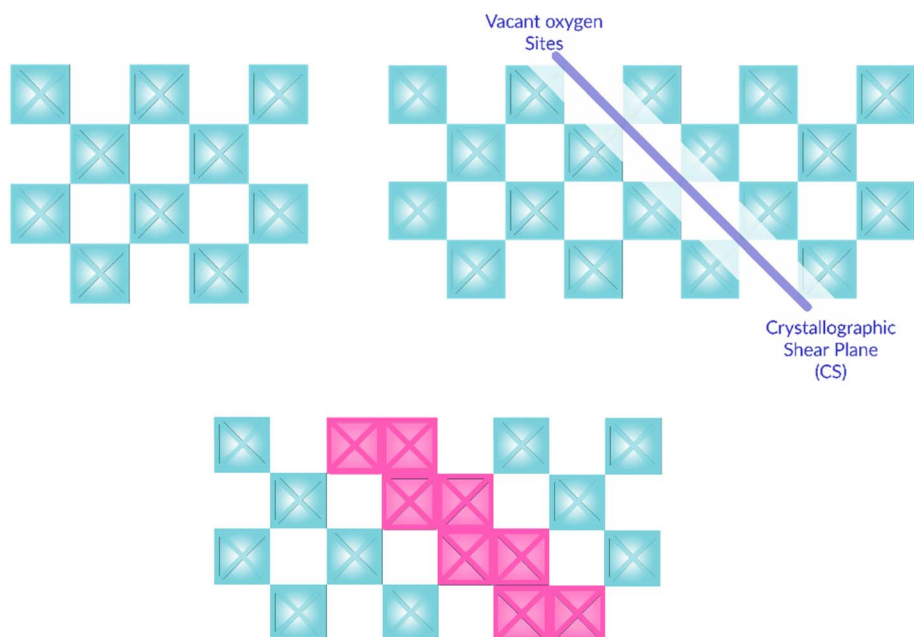


Fig. 2 Formation of Wadsley–Roth block structures from (a)  $\text{ReO}_3$ -like blocks and (b) the introduction of a crystallographic shear plane, to result in a (c) block structure.



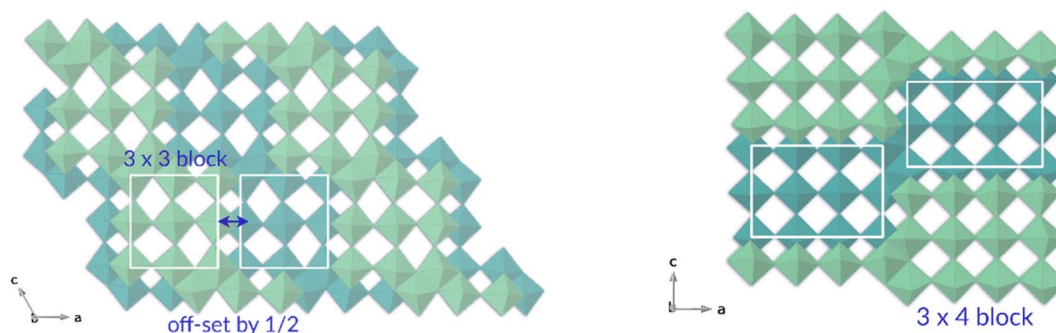


Fig. 3 Crystal structure of  $\text{TiNb}_2\text{O}_7$  (left) and  $\text{Ti}_2\text{Nb}_{10}\text{O}_{29}$  (right).

Li in solution can then be recovered as Li salts for potential use in the synthesis of Li ion battery cathode materials.

## Experimental

### Proton exchange

Three acids were investigated for the effectiveness of the  $\text{H}^+/\text{Li}^+$  exchange in LTO:  $\text{HCl}$ ,  $\text{H}_2\text{SO}_4$ ,  $\text{H}_3\text{PO}_4$ . 2 g of LTO (Gelon) was dispensed and added to a 45 mL Teflon liner with 20 mL of 2 M acid. The Teflon liner was placed in a steel autoclave, which was heated at 150 °C for 24 hours in an oven. The resulting mixture was filtered, with the sample being washed with excess water (<100 mL) to allow for the full removal of the solid residue from the Teflon liner. The collected solid was then dried at 60 °C before X-ray diffraction characterisation. Before use of the recovered  $\text{TiO}_2$  in the synthesis of the Ti–Nb–O phases below, the powder was further heated to 600 °C for 1 h to ensure loss of any water of hydration.

### Concentration step

The excess water removal and concentration of the solutions to <5 mL was conducted *via* rotary evaporation. This concentration step results in the precipitation of the lithium salt.

### Synthesis of $\text{TiNb}_2\text{O}_7$ from $\text{Li}^+$ exchanged pristine LTO

The recovered  $\text{TiO}_2$  and  $\text{Nb}_2\text{O}_5$  (Alfa Aesar; 99.5%; T-phase) were ground in appropriate stoichiometric ratios in an Agate pestle and mortar, before being transferred into a Fritsch planetary Pulverisette 7 and milled for 1 h/300 rpm in a zirconia milling jar with three 10 mm zirconia balls, before heating in an alumina crucible up to 1300 °C for 15 h, at a ramp rate of 5 °C  $\text{min}^{-1}$  under air.

### Synthesis of $\text{Ti}_2\text{Nb}_{10}\text{O}_{29}$ from $\text{Li}^+$ exchanged pristine LTO

The recovered  $\text{TiO}_2$  and  $\text{Nb}_2\text{O}_5$  (Alfa Aesar; 99.5%; T-phase) were ground in appropriate stoichiometric ratios in an Agate pestle and mortar. The mixture was heated in an alumina crucible up to 1100 °C for 12 hours, at a ramp rate of 5 °C  $\text{min}^{-1}$ . The sample was re-ground and re-heated once again under the same conditions.

### Phase purity

The phase purity of the recovered  $\text{TiO}_2$ , Li salts and upcycled Ti–Nb–O phases were evaluated using Powder X-ray Diffraction (PXRD) (Bruker D8 diffractometer (Cu  $\text{K}_\alpha$ ) or Bruker D2 diffractometer (Co  $\text{K}_\alpha$ )).

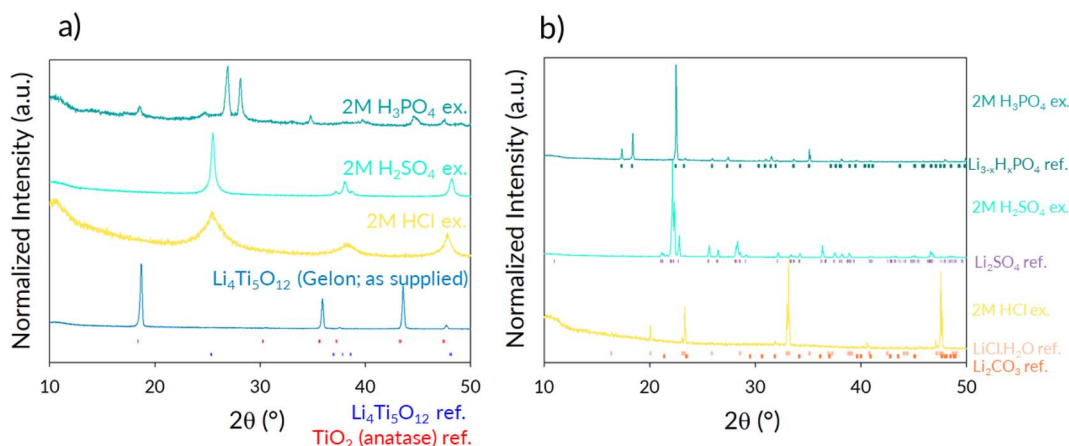


Fig. 4 (a) XRD patterns of pristine LTO (Gelon) and the obtained solids after acid exchange with 2 M:  $\text{HCl}$ ,  $\text{H}_2\text{SO}_4$ , and  $\text{H}_3\text{PO}_4$ . Reference plots of LTO and  $\text{TiO}_2$  (anatase) are added. (b) XRD patterns of the crystals obtained from the LTO-acid exchanged solutions. Reference plots of  $\text{Li}_3\text{xH}_\text{x}\text{PO}_4$ ,  $\text{Li}_2\text{SO}_4$ ,  $\text{LiClH}_2\text{O}$ , and  $\text{Li}_2\text{CO}_3$  are added.



**Table 1** The Li<sup>+</sup> content directly extracted from the LTO-acid exchange solutions using 2 M acid solutions

Acid type	Theoretical mass of Li (g)	Extracted Li content (g)	Extraction of Li%
2 M HCl	0.1217	0.120 (3)	99 (2)
2 M H <sub>2</sub> SO <sub>4</sub>	0.1220	0.124 (5)	102 (4)
2 M H <sub>3</sub> PO <sub>4</sub>	0.1221	0.084 (2)	69 (2)

### Inductively coupled plasma – optical emission spectrometry (ICP-OES) analysis

The acid lithium-leached samples were analysed using an Agilent 5110 ICP-OES with an argon plasma torch (Agilent Technologies, USA). Three repeat measurements were taken for each individual sample by the instrument with a rinse step between each sample. To overcome any drift with time due to the temperature of the instrument, the 0, 5, 20 and 70 ppm standards were remeasured every 20 samples, and a re-slope of the calibration line performed. An error of 20% and an  $r^2$  value of 0.995 were chosen for the calibration lines.

For the axial standards (0–15 ppm), a 50 ppm working solution was prepared from elemental stock solution set at 1000 ppm. This working solution was appropriately diluted down to produce the desired standards using volumetric flasks. These standards were acidified using aqua regia.

For the radial standards (20–100 ppm), these standards were prepared individually (rather than previous, where a working solution of 50 ppm was used) using elemental stock solution standards at 1000 ppm to create the desired concentrations. These were also acidified using aqua regia.

### Coating and cell fabrication

The electrode ink coating was formulated with an 80 : 10 : 10 ratio of active material, carbon black, and binder (polyvinylidene difluoride – PVDF) using a Thinky Mixer. Initially, the binder (PVDF) was mixed with *N*-methyl pyrrolidone (NMP) for 5 minutes at 1300 rpm. Subsequently, SuperP carbon black and the active material were added, and at each step the mixture was mixed for 10 minutes at 1300 rpm, with additional NMP added as necessary to create a slurry. The mixture was then

degassed for 3 minutes at 1800 rpm. The resulting slurry was coated on aluminium foil using a draw-down coater, setting the bar height to 200 μm. After coating, the material was dried at 80 °C for up to 2 h and then transferred to a vacuum oven set at 110 °C for overnight drying. Calendering was performed between two stainless steel rollers at 80 °C until the coated material's porosity reached approximately 30–40%.

In an argon-filled glovebox, Li-half cells were fabricated. Circular disks (12 mm) of the coated active material were weighed outside the glovebox before being transferred inside. For assembly, steel 2032 cases were used with a single 1 mm stainless steel spacer for compression. The lithium metal electrode was prepared from lithium ribbon, and its surface was scratched using a stainless steel spatula to achieve a shiny and rough texture before cutting it to size (12.7 mm). The electrolyte used was 1.0 M LiPF<sub>6</sub> in a 50 : 50 (v/v) mixture of ethylene carbonate and dimethyl carbonate, with two 50 μL additions made during assembly. The glass fibre separator was cut to size (14.3 mm) for incorporation into the cell.

### Electrochemical testing

The electrochemical performances of the synthesised Ti–Nb–O phases were evaluated using a BioLogic BCS805 battery tester, with the cells cycled between 1.0 and 2.5 V in galvanostatic mode. All cells had three formation cycles applied with a current density of 0.01 A g<sup>-1</sup> between the two voltage limits. A constant voltage step was applied on lithiation, where the lower voltage limit was held for 3 h or until the current reached 40%. A rest of 10 minutes was also applied between each cycle.

Asymmetric cell testing was applied to each cell such that 0.1 A g<sup>-1</sup> was constantly being applied during lithiation, with a 40% current breakdown limit or 3 h hold. The delithiation rate gradually increased from: 0.1, 0.2, 0.4, 0.6, 1, 2 and 4 A g<sup>-1</sup> with 5 cycles at each rate step. Asymmetric cycling was introduced to limit the current rate limitations created using Li metal in an organic electrolyte.<sup>44,45</sup> After the rate study 5 more cycles were performed at 0.1 A g<sup>-1</sup>.

Triplicate data were collected for each measurement under the same conditions to deduce the average (de)lithiation capacities and the standard deviation associated with these values (given in parentheses in the text). The average mass

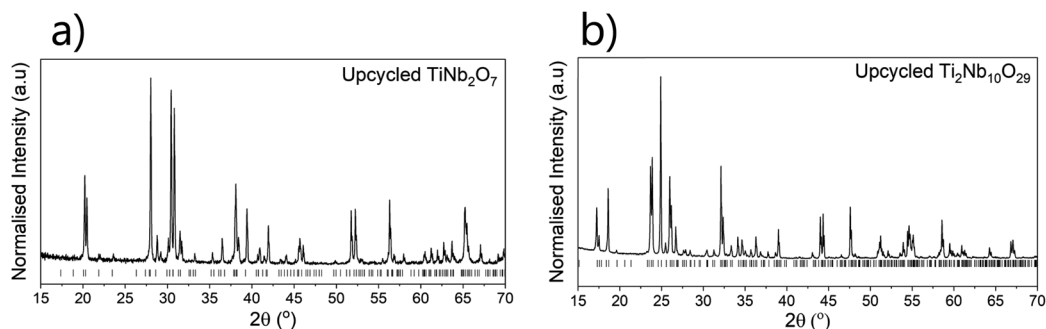


**Fig. 5** (a) PXRD pattern of upcycled TiNb<sub>2</sub>O<sub>7</sub> (Co K $\alpha$ ), with the peak positions for monoclinic TiNb<sub>2</sub>O<sub>7</sub> shown with black dashes. (b) PXRD patterns of upcycled Ti<sub>2</sub>Nb<sub>10</sub>O<sub>29</sub> (Cu K $\alpha$ ) and the peak positions for orthorhombic Ti<sub>2</sub>Nb<sub>10</sub>O<sub>29</sub>.





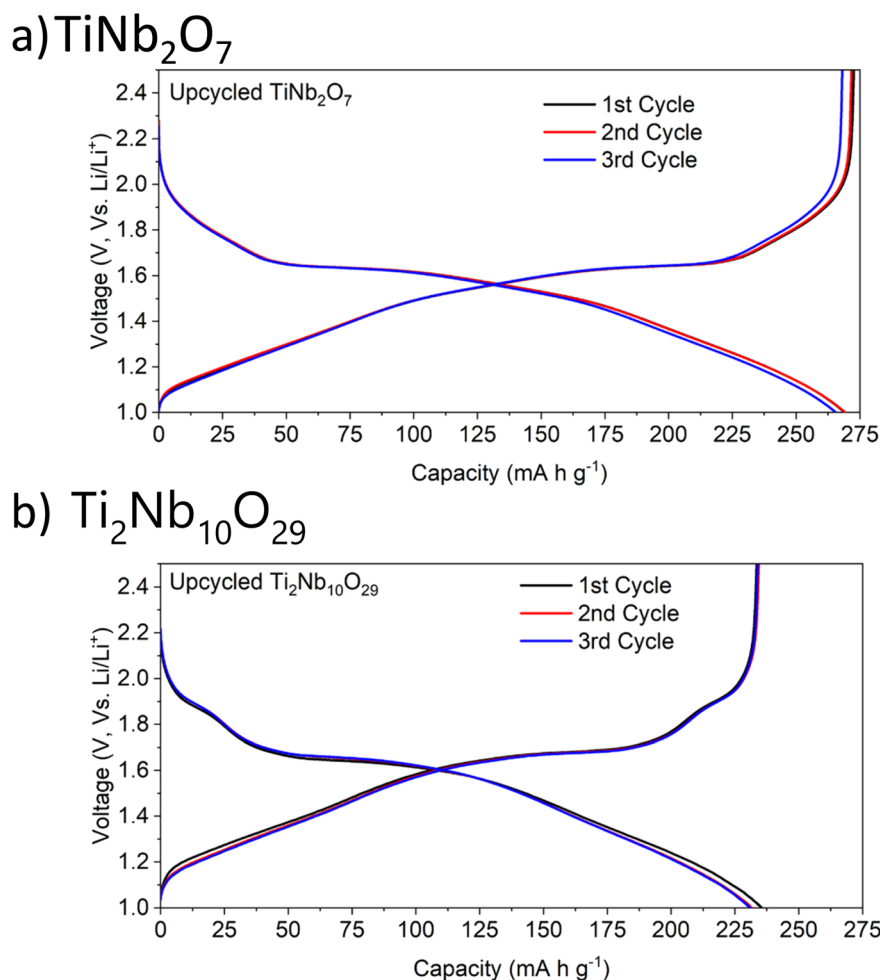


Fig. 6 Galvanostatic discharge–charge curves of (a) upcycled  $\text{TiNb}_2\text{O}_7$  and (b) upcycled  $\text{Ti}_2\text{Nb}_{10}\text{O}_{29}$  with a current density of  $10 \text{ mA g}^{-1}$  applied between voltage limits between 1 to 2.5 V.

loading for the upcycled  $\text{TiNb}_2\text{O}_7$  (TNO) was  $3.1 (2) \text{ mg cm}^{-2}$  and  $\text{Ti}_2\text{Nb}_{10}\text{O}_{29}$  was  $4.3 (2) \text{ mg cm}^{-2}$ .

Long term cycling for both upcycled materials was performed using a BioLogic BCS805 battery tester, with the cell being cycled between 1.0 and 2.5 V in galvanostatic mode. 100 cycles at  $0.2 \text{ A g}^{-1}$  were performed for each cell.

## Results and discussion

### Lithium extraction

Initial work focused on evaluating the potential for  $\text{H}^+/\text{Li}^+$  exchange in LTO, in order to allow the recovery of Li, which represents the most valuable component of this electrode. Assuming complete exchange of the  $\text{Li}^+$  from LTO, for every 2 g of LTO, 0.122 g would be associated to the Li mass – however the extraction of the  $\text{Li}^+$  is dependent on its counter ion and hence solubility (a chart highlighting a variety of lithium salts solubility vs. temperature can be seen in ESI Fig. 1†).

The complete exchange of  $\text{Li}^+$  by  $\text{H}^+$  was successful with the 2 M acids HCl and  $\text{H}_2\text{SO}_4$ , leading to recovery of  $\text{TiO}_2$  (anatase) from the pristine LTO, as shown in Fig. 4a, with the Li leached into solution. This is also reinforced by the ICP-OES data for the

leached solutions, which show complete exchange (within errors) with both acids (Table 1). In contrast to the above results, the use of  $\text{H}_3\text{PO}_4$  produces a mixture of anatase along with an alternative phase ( $\text{LiTiOPO}_4$ ), which has been recently studied as a possible anode in LIBs.<sup>46–48</sup> As a result of the presence of this alternative Li containing phase, the Li leaching is incomplete for this acid. The ICP-OES results confirm the successful lithium exchange, and while excess water was used to remove the samples from the autoclaves, commercially a more direct and efficient process could be implemented to reduce this and so limit the concentration step required to recover the salts (photographs of the concentrated solutions are shown in ESI Fig. 2†). To confirm the nature of the lithium salts from the acid exchange, crystals from the solutions were obtained and analysed using PXRD, and the resulting patterns are shown in Fig. 4b. While the phosphoric acid may not fully remove all the lithium from LTO (due to the formation of  $\text{LiTiOPO}_4$ ),  $\text{Li}_{3-x}\text{H}_x\text{PO}_4$  was identified. For the  $\text{H}_2\text{SO}_4$  and HCl exchanges,  $\text{Li}_2\text{SO}_4$  and  $\text{LiCl}\cdot\text{H}_2\text{O}$  were both detected respectively, although in the latter, it is believed  $\text{Li}_2\text{CO}_3$  may also be present (*ca.*  $31.8^\circ 2\theta$ ) – which may result from air exposure from drying overnight. Rather than precipitating these particular salts, these lithium



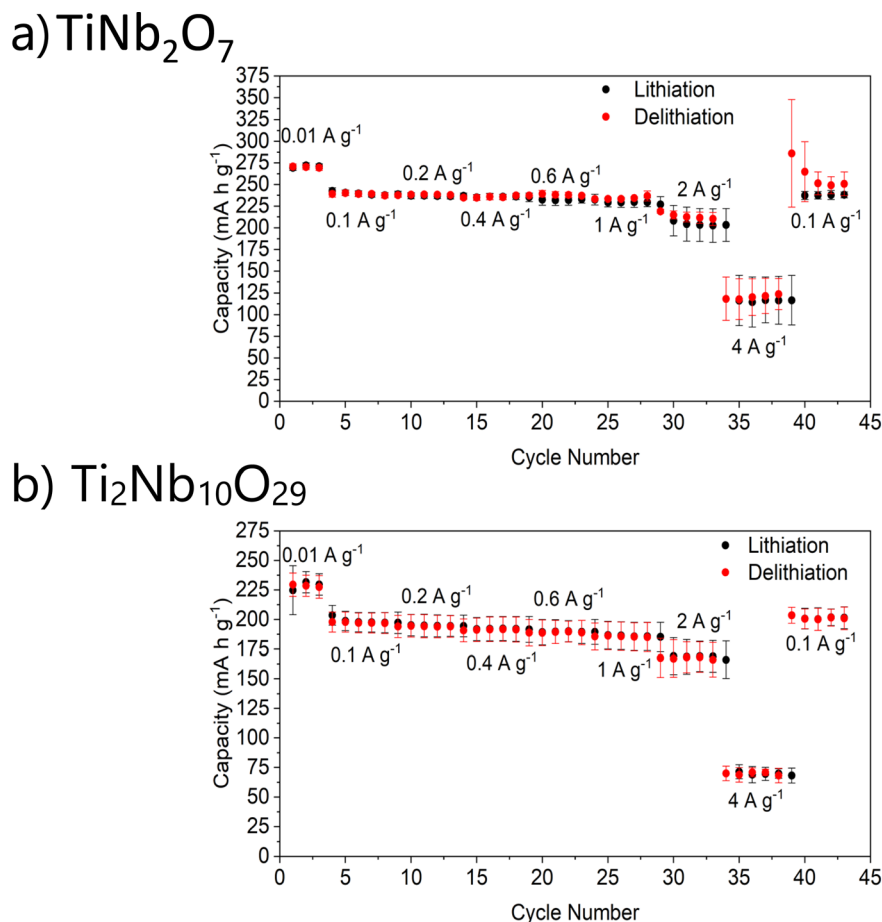


Fig. 7 Average specific capacities of three upcycled  $\text{TiNb}_2\text{O}_7$  cells (a) and three upcycled  $\text{Ti}_2\text{Nb}_{10}\text{O}_{29}$  cells (b) undergoing asymmetric cycling – such that the lithiation current density is maintained at  $0.1 \text{ A g}^{-1}$ , while the delithiation gradually increases after 5 cycles at each rate step. The red error bars are for lithiation, the black for the delithiation. The higher delithiation capacities on returning to  $0.1 \text{ A g}^{-1}$  after the rate tests, in the TNO cells, relate to a use of Li metal counter electrode: lithium dendrites having formed, and therefore higher charging capacities due to soft shorting.

salt solutions could be used in further processing to form lithium hydroxide or carbonate, which are common reagents for cathode synthesis.

### LTO upcycling to $\text{Ti}_2\text{Nb}_{10}\text{O}_{29}$ and $\text{TiNb}_2\text{O}_7$

The recovered anatase was then used to synthesise two common titanium-doped niobate anodes,  $\text{TiNb}_2\text{O}_7$  and  $\text{Ti}_2\text{Nb}_{10}\text{O}_{29}$ , and phase purity characterised with XRD (Fig. 5). The  $\text{TiNb}_2\text{O}_7$  phase was found to contain a small amount of  $\text{Ti}_2\text{Nb}_{10}\text{O}_{29}$  as an impurity. This is common in the synthesis of this material.<sup>49</sup> Furthermore, its' presence in small amounts has been reported to give a small improvement in rate capability, and so such mixed compositions have been patented.<sup>49</sup>

The electrochemical rate performance of the upcycled Ti–Nb–O systems were assessed through asymmetric cycling in the 1–2.5 V window after 3 formation cycles at  $10 \text{ mA g}^{-1}$  (Fig. 6). The upcycled  $\text{TiNb}_2\text{O}_7$ 's first discharge capacity was found to be  $272 (3) \text{ mA h g}^{-1}$ , followed by a capacity  $271 (3)$  and  $268 (3) \text{ mA h g}^{-1}$  for the second and third cycle – giving a 99% capacity retention on formation. An equivalent formation capacity retention is found for  $\text{Ti}_2\text{Nb}_{10}\text{O}_{29}$  with an initial

discharge capacity of  $232 (9) \text{ mA h g}^{-1}$ , followed by  $231 (8)$  and  $228 (9) \text{ mA h g}^{-1}$  for the second and third cycle, respectively. The difference in the capacities of these two materials can be attributed to their relative molecular mass, which would impact the gravimetric capacity. Following the initial formation rates, the lithiation rate was kept constant at  $0.1 \text{ A g}^{-1}$  whilst the delithiation rate gradually increased from  $0.1 \text{ A g}^{-1}$  to  $4 \text{ A g}^{-1}$ . The rate performance for each material was tested and is shown in Fig. 7 for both upcycled materials.

For both materials significant capacity retention is observed between rates  $0.1$  and  $4 \text{ A g}^{-1}$ . Both upcycled materials showed high gravimetric capacities at  $2 \text{ A g}^{-1}$  (corresponding to *ca.* 7.4 C for  $\text{TiNb}_2\text{O}_7$  and *ca.* 8.6 C for  $\text{Ti}_2\text{Nb}_{10}\text{O}_{29}$ ), with the average capacity for  $\text{TiNb}_2\text{O}_7$  at  $219 (2) \text{ mA h g}^{-1}$  and  $\text{Ti}_2\text{Nb}_{10}\text{O}_{29}$  at  $168 (16) \text{ mA h g}^{-1}$ . At  $4 \text{ A g}^{-1}$  (corresponding to *ca.* 14.7 C for  $\text{TiNb}_2\text{O}_7$  and *ca.* 17.3 C for  $\text{Ti}_2\text{Nb}_{10}\text{O}_{29}$ ) there is a large drop in capacity for both materials with the average capacity for  $\text{TiNb}_2\text{O}_7$  and  $\text{Ti}_2\text{Nb}_{10}\text{O}_{29}$  at  $118 (25) \text{ mA h g}^{-1}$  and  $70 (6) \text{ mA h g}^{-1}$ , respectively. After completing the asymmetric rate study, a subsequent 5 cycles were performed at  $0.1 \text{ A g}^{-1}$  showing that the low rate capacity could be recovered. Interestingly, for  $\text{Ti}_2\text{Nb}_{10}\text{O}_{29}$  the capacity recovered to 204



(6) mA h g<sup>-1</sup> which is slightly higher than the original capacity at this rate, thus indicating that further optimisation of the formation cycles may be needed to enhance the performance. The recovery in the capacities for both materials indicate that the high rates applied to them during this rate study did not negatively affect the performance of the materials. The capacities observed for both upcycled materials are similar to the pristine materials, as seen in the literature, indicating that this upcycling process is a promising route to these materials.<sup>50–55</sup>

After the rate test, long term cycling was performed on both materials at 0.2 A g<sup>-1</sup> for 100 cycles. Both upcycled materials showed a good capacity retention over 100 cycles at ca. 98%. The long term cycling data for both upcycled materials is presented in ESI Fig. 3 and 4,† in addition the SEM images collected of the pristine material and the corresponding morphology post-cycling (ESI Fig. 5†).

## Conclusions

In summary, we have reported an approach to upcycle LTO whilst also recovering the Li as Li salts. By using HCl and H<sub>2</sub>SO<sub>4</sub>, complete H<sup>+</sup>/Li<sup>+</sup> exchange is possible giving pure anatase which can be used to upcycle into TiNb<sub>2</sub>O<sub>7</sub> and Ti<sub>2</sub>Nb<sub>10</sub>O<sub>29</sub>. The Li can then be recovered as Li<sub>2</sub>SO<sub>4</sub> and LiCl·H<sub>2</sub>O thus highlighting the process as a route to recover a valuable Li resource stream. In contrast, using H<sub>3</sub>PO<sub>4</sub> led to the formation of anatase and an alternative phase (LiTiOPO<sub>4</sub>), preventing the complete exchange of Li, although this leached Li could then be covered as lithium phosphate.

From the electrochemical testing, within a Li-half cell, the upcycled materials show high capacity and rate capability between 0.1 and 2 A g<sup>-1</sup>, demonstrating their potential as high-power anodes, and thus illustrating this route as a potential means of recycling LTO with lithium recovery and upcycling to next generation high-power anodes.

## Data availability

Data sets available: DOI: <https://doi.org/10.25500/edata.bham.00001058>.

## Author contributions

Alex J. Green: investigation, data curation, formal analysis, visualization, writing – original draft, writing – review and editing. Elizabeth H. Driscoll: investigation, methodology, data curation, formal analysis, visualization, writing – original draft, writing – review and editing. Paul Anderson; supervision, funding, resources, and writing – review and editing. Emma Kendrick: supervision, funding, resources, and writing – review and editing. Peter R. Slater: conceptualization, funding, methodology, supervision, resources, writing – original draft, and writing – review and editing.

## Conflicts of interest

There are no conflicts to declare.

## Acknowledgements

We would like to thank Faraday Institution: FITG045 (AJG studentship), CATMAT (FIRG016), ReLiB (FIRG027), and NEX-TRODE (FIRG015) projects for funding.

## References

- 1 A. T. Sargent, Z. Henderson, A. S. Walton, B. F. Spencer, L. Sweeney, W. R. Flavell, P. A. Anderson, E. Kendrick, P. R. Slater and P. K. Allan, *J. Mater. Chem. A*, 2023, **11**, 9579–9596.
- 2 G. Harper, R. Sommerville, E. Kendrick, L. Driscoll, P. Slater, R. Stolkin, A. Walton, P. Christensen, O. Heidrich, S. Lambert, A. Abbott, K. Ryder, L. Gaines and P. Anderson, *Nature*, 2019, **575**, 75–86.
- 3 W. Lv, Z. Wang, H. Cao, Y. Sun, Y. Zhang and Z. Sun, *ACS Sustain. Chem. Eng.*, 2018, **6**, 1504–1521.
- 4 R. Sommerville, J. Shaw-Stewart, V. Goodship, N. Rowson and E. Kendrick, *Sustainable Mater. Technol.*, 2020, **25**, e00197.
- 5 Y. Bai, N. Muralidharan, Y.-K. Sun, S. Passerini, M. Stanley Whittingham and I. Belharouak, *Mater. Today*, 2020, **41**, 304–315.
- 6 G. D. J. Harper, E. Kendrick, P. A. Anderson, W. Mroziak, P. Christensen, S. Lambert, D. Greenwood, P. K. Das, M. Ahmeid, Z. Milojevic, W. Du, D. J. L. Brett, P. R. Shearing, A. Rastegarpanah, R. Stolkin, R. Sommerville, A. Zorin, J. L. Durham, A. P. Abbott, D. Thompson, N. D. Browning, B. L. Mehdi, M. Bahri, F. Schanider-Tontini, D. Nicholls, C. Stallmeister, B. Friedrich, M. Sommerfeld, L. L. Driscoll, A. Jarvis, E. C. Giles, P. R. Slater, V. Echavarrri-Bravo, G. Maddalena, L. E. Horsfall, L. Gaines, Q. Dai, S. J. Jethwa, A. L. Lipson, G. A. Leeke, T. Cowell, J. G. Farthing, G. Mariani, A. Smith, Z. Iqbal, R. Golmohammadzadeh, L. Sweeney, V. Goodship, Z. Li, J. Edge, L. Lander, V. T. Nguyen, R. J. R. Elliot, O. Heidrich, M. Slattery, D. Reed, J. Ahuja, A. Cavoski, R. Lee, E. Driscoll, J. Baker, P. Littlewood, I. Styles, S. Mahanty and F. Boons, *JPhys Energy*, 2023, **5**, 021501.
- 7 P. Zhu, E. H. Driscoll, B. Dong, R. Sommerville, A. Zorin, P. R. Slater and E. Kendrick, *Green Chem.*, 2023, **25**, 3503–3514.
- 8 B. Zhao, R. Ran, M. Liu and Z. Shao, *Mater. Sci. Eng., R*, 2015, **98**, 1–71.
- 9 H. Zhang, Y. Yang, H. Xu, L. Wang, X. Lu and X. He, *InfoMat*, 2022, **4**, e12228.
- 10 E. Ferg, R. J. Gummow, A. de Kock and M. M. Thackeray, *J. Electrochem. Soc.*, 1994, **141**, 147–150.
- 11 X. Bai, T. Li, C. Wei, Y. K. Sun, Y. X. Qi, H. L. Zhu, N. Lun and Y. J. Bai, *Electrochim. Acta*, 2015, **155**, 132–139.
- 12 A. D. Robertson, L. Trevino, H. Tukamoto and J. T. S. Irvine, *J. Power Sources*, 1999, **81–82**, 352–357.
- 13 C. H. Chen, J. T. Vaughey, A. N. Jansen, D. W. Dees, A. J. Kahaian, T. Goacher and M. M. Thackeray, *J. Electrochem. Soc.*, 2001, **148**, A102.
- 14 Y. J. Hao, Q. Y. Lai, J. Z. Lu and X. Y. Ji, *Ion*, 2007, **13**, 369–373.



- 15 Y. J. Bai, C. Gong, N. Lun and Y. X. Qi, *J. Mater. Chem. A*, 2012, **1**, 89–96.
- 16 M. M. Thackeray and K. Amine, *Nat. Energy*, 2021, **6**, 683.
- 17 C. Pillot, presented in part at the Batteries Event 2021, Avicenne Energy, Lyon, September 2021.
- 18 M. Baumann, J. F. Peters, M. Weil and A. Grunwald, *Energy Technol.*, 2017, **5**, 1071–1083.
- 19 Toshiba researchers use TiNb<sub>2</sub>O<sub>7</sub> anodes for high-energy, fast-charging, long-life Li-ion batteries for EVs – Green Car Congress, <https://www.greencarcongress.com/2018/07/20180706-toshiba.html>, accessed 24 July 2023.
- 20 K. Nakahara, T. Seki, H. Ishioka, W. Mino, Y. Harada, N. Takami, H. Inagaki, *US Pat.*, US20150243979A1, 2014.
- 21 N. Takami, K. Ise, Y. Harada, T. Iwasaki, T. Kishi and K. Hoshina, *J. Power Sources*, 2018, **396**, 429–436.
- 22 X. Wu, J. Miao, W. Han, Y.-S. Hu, D. Chen, J.-S. Lee, J. Kim and L. Chen, *Electrochem. Commun.*, 2012, **25**, 39–42.
- 23 K. J. Griffith, A. Senyshyn and C. P. Grey, *Inorg. Chem.*, 2017, **56**, 4002–4010.
- 24 C. Yang, S. Deng, C. Lin, S. Lin, Y. Chen, J. Li and H. Wu, *Nanoscale*, 2016, **8**, 18792–18799.
- 25 H. Aghamohammadi, N. Hassanzadeh and R. Eslami-Farsani, *J. Alloys Compd.*, 2022, **911**, 165117.
- 26 J.-T. Han, Y.-H. Huang and J. B. Goodenough, *Chem. Mater.*, 2011, **23**, 2027–2029.
- 27 T. Jiang, S. Ma, J. Deng, T. Yuan, C. Lin and M. Liu, *Adv. Sci.*, 2022, **9**, 2105119.
- 28 O. A. Drozhzhin, V. V. Grigoryev, A. M. Alekseeva, R. R. Samigullin, D. A. Aksyonov, O. V. Boytsova, D. Chernyshov, V. V. Shapovalov, A. A. Guda, A. V. Soldatov, K. J. Stevenson, A. M. Abakumov and E. V. Antipov, *ACS Appl. Mater. Interfaces*, 2021, **13**, 56366–56374.
- 29 A. J. Green, E. H. Driscoll, Y. Lakhdar, E. Kendrick and P. R. Slater, *Dalton Trans.*, 2023, **52**, 13110–13118.
- 30 Y. Yang and J. Zhao, *Adv. Sci.*, 2021, **8**, 202004855.
- 31 B. D. Sten Andersson and D. A. D Wadsley, *Nature*, 1966, **211**, 581–583.
- 32 R. J. Cava, D. W. Murphy and S. M. Zahurak, *J. Electrochem. Soc.*, 1983, **130**, 2345–2351.
- 33 K. J. Griffith, I. D. Seymour, M. A. Hope, M. M. Butala, L. K. Lamontagne, M. B. Preefer, C. P. Koçer, G. Henkelman, A. J. Morris, M. J. Cliffe, S. E. Dutton and C. P. Grey, *J. Am. Chem. Soc.*, 2019, **141**, 16706–16725.
- 34 C. P. Koçer, K. J. Griffith, C. P. Grey and A. J. Morris, *J. Am. Chem. Soc.*, 2019, **141**, 15121–15134.
- 35 G. Liu, C. Li, H. Zhou, H. Tang, G. Long, L. Wei, *CN Pat.*, CN102390863B, 2011.
- 36 European Commission, [https://ec.europa.eu/growth/sectors/raw-materials/areas-specific-interest/critical-raw-materials\\_en](https://ec.europa.eu/growth/sectors/raw-materials/areas-specific-interest/critical-raw-materials_en), accessed 25 October 2021.
- 37 L. da Silva Lima, J. Wu, E. Cadena, A. S. Groombridge and J. Dewulf, *Sustainable Mater. Technol.*, 2023, **37**, e00654.
- 38 D. Etienne, W. Lisa, D. Laetitia, S. N. Bookhari, S. A. Abdullah, M. K. Hussein, D. B. Agusdinata, W. Liu, H. Eakin and H. Romero, *Environ. Res.*, 2018, **13**, 123001.
- 39 How lithium mining is fueling the EV revolution | McKinsey, <https://www.mckinsey.com/industries/metals-and-mining/our-insights/lithium-mining-how-new-production-technologies-could-fuel-the-global-ev-revolution>, accessed 24 July 2023.
- 40 W. Liu and D. B. Agusdinata, *J. Cleaner Prod.*, 2020, **260**, 120838.
- 41 A. R. Alves and A. d. R. Coutinho, *Miner. Eng.*, 2019, **132**, 275–283.
- 42 Brazil: niobium mine production | Statista, <https://www.statista.com/statistics/1025809/brazil-niobium-mine-production/>, accessed 24 July 2023.
- 43 CRMS 2023 – SCRREEN2, <https://screen.eu/crms-2023/>, accessed 20 July 2023.
- 44 Y. Lakhdar, H. Geary, M. Houck, D. Gastol, A. S. Groombridge, P. R. Slater and E. Kendrick, *ACS Appl. Energy Mater.*, 2022, **5**, 11229–11240.
- 45 Y. Lakhdar, Y. Chen, H. Geary, M. E. Houck, A. S. Groombridge, P. R. Slater and E. Kendrick, *J. Power Sources*, 2023, **588**, 233710.
- 46 Y. Fu, H. Ming, S. Zhao, J. Guo, M. Chen, Q. Zhou and J. Zheng, *Electrochim. Acta*, 2015, **185**, 211–217.
- 47 X. Gu, Y. Cai, X. Yao, H. Tian and Z. Su, *ChemistrySelect*, 2023, **8**, e202203329.
- 48 X. Li, Y. Cai, X. Yao, H. Tian and Z. Su, *Mater. Lett.*, 2023, **346**, 134542.
- 49 N. Kiyoshi, S. Toshimasa, I. Hidenori, M. Wataru, H. Yasuhiro, T. Norio and I. Hiroki, *EP Pat.*, EP2911223B1, 2015.
- 50 R. Tao, T. Zhang, X. G. Sun, C. L. Do-Thanh and S. Dai, *Batteries Supercaps*, 2023, **6**, e202300101.
- 51 X. Zhang, Z. Zhang, J. Zhang, W. Mao, K. Bao and Y. Qian, *Inorg. Chem. Commun.*, 2023, **151**, 110422.
- 52 S. Gong, Y. Wang, Q. Zhu, M. Li, Y. Wen, H. Wang, J. Qiu and B. Xu, *J. Power Sources*, 2023, **564**, 232672.
- 53 W. Utetiwabo, M. Khurram Tufail, C. Zeng, L. Zhou, L. Yang, Z. Hua, J. Zeng, P. Yu, R. Shao and W. Yang, *J. Colloid Interface Sci.*, 2022, **623**, 1015–1026.
- 54 H. Li, X. Cai, J. Li, C. Deng, Y. Liu, H. Yan, H. Yu, L. Zhang, M. Shui, L. Yan and J. Shu, *Ceram. Int.*, 2022, **48**, 23334–23340.
- 55 C. Deng, J. Xu, H. Yu, Y. Liu, X. Cai, H. Yan, L. Fan, M. Shui, L. Yan and J. Shu, *Ceram. Int.*, 2022, **48**, 33200–33207.

